Available online at www.sciencedirect.com
ScienceDirect
International Journal of Heat and Mass Transfer 51 (2008) 5443–5453
International Journal of HEAT and MASS TRANSFER
www.elsevier.com/locate/ijhmt

Design of a deflected membrane electrode assembly for PEMFCs

Dewan Hasan Ahmed, Hyung Jin Sung *

Department of Mechanical Engineering, KAIST, 373-1, Guseong-dong Yuseong-gu, Daejeon 305-701, Republic of Korea

Received 12 December 2006; received in revised form 22 August 2007
Available online 28 April 2008

Abstract

Simulations were performed of a proton exchange membrane fuel cell (PEMFC) in which the membrane electrode assembly (MEA) was deflected such that the adjacent shoulders of the channel assembly were at different heights. The effect on cell performance of varying the MEA deflection was examined while maintaining the same reacting area and boundary conditions at high operating current densities. A three-dimensional, non-isothermal model was employed with a single straight channel. Both humidification and phase transportation were included in the model to obtain the total water management for systems operating at different current densities. The cell performance was found to increase significantly at a certain, optimal deflection. The cathode overpotential decreased significantly with increasing MEA deflection as the reactants became more evenly distributed over the reacting area. A preliminary investigation of the deflection behavior of different MEA materials under clamping pressures taken from the literature indicated that MEA materials can be deflected up to the optimal deflection condition provided the clamping pressure is within the elastic limit of the gas diffusion electrode (GDE).

Keywords: PEMFC; High current density; Deflection; Channel–shoulder width ratio; Cathode overpotential; Ohmic loss

1. Introduction

Optimizing the geometrical design of proton exchange membrane fuel cells (PEMFCs) is a major issue in efforts to commercialize these cells. In PEMFCs, fuel and oxidant struggle to reach the shoulder region, and water removal from that region to the channel area is a key issue as the water produced in the oxidation reaction congests the pores of the gas diffusion layer (GDL) and increases the concentration losses. The clamping of the two bipolar plates also reduces the permeability and porosity of gas diffusion layer (GDL) in the shoulder region, a problem that is particularly severe in the downstream region of the channel, especially when the system is operated at high current density. Many efforts have been made to improve cell performance, concentrating on different aspects of PEMFCs. Among the various aspects of PEMFCs that affect cell performance, geometrical parameters play a major role. To date, the channel and shoulder widths have received particular attention from researchers. It has been found that cells with smaller shoulder widths (compared with the channel width) perform better than those with larger shoulder widths [1–4]. A small shoulder width helps to reduce concentration losses by diffusing more reactants to the reacting area under the shoulder, and also facilitates the removal of water produced by chemical reaction. Other modifications of the PEMFC geometry have also been investigated in efforts to achieve effective distribution of the reactants to the reacting area through the gas diffusion layer, including varying the flow field (e.g., using a serpentine, integrated flow field) [5,6], introducing baffles in the channel area [7], and using a converging channel cross-section [8]. In addition, an improvement in PEMFC performance was observed using a trapezoidal channel cross-section, in which the channel face width increases by comparison with the rectangular or square channel cross-section [9]. Much of the previous work in this area has focused on achieving uniform reaction over the reacting area by

* Corresponding author. Tel.: +82 42 869 3027; fax: +82 42 869 5027.
E-mail address: hjsung@kaist.ac.kr (H.J. Sung).

0017-9310/$ - see front matter © 2008 Elsevier Ltd. All rights reserved.
doi:10.1016/j.ijheatmasstransfer.2007.08.037

Nomenclature

A_{cv}	specific surface area of the control volume, m^{-1}
$Area_{cv}$	surface area of the control volume, m^2
C_{wa}	concentration of water vapor at the anode, mol m^{-3}
C_{wc}	concentration of water vapor at the cathode, mol m^{-3}
$D_{H_2,l}$	diffusion coefficient of H_2 in a liquid water film, 6.3×10^{-9} m^2 s^{-1}
$D_{O_2,l}$	diffusion coefficient of O_2 in a liquid water film, 2.4×10^{-9} m^2 s^{-1}
D_W	diffusion coefficient of water, m^2 s^{-1}
F	Faraday constant, 96,487 C $mole^{-1}$
H	channel height, m
$H_{H_2,l}$	Henry's law constant for H_2 in a liquid water film, 8.9×10^9 Pa
$H_{O_2,l}$	Henry's law constant for O_2 in a liquid water film, 2.12×10^{10} Pa
h_{rxn}	enthalpy of water formation, kJ K mol^{-1}
h_{fg}	enthalpy of vaporization of water, kJ kg^{-1}
I	local current density, A m^{-2}
I_{avg}	average current density, A m^{-2}
$I_{0,K}$	exchange current density for reaction K, A m^{-2}
L	length, m
l	distance between two applied forces (in Fig. 13), m
$M_{m,dry}$	equivalent weight of a dry membrane, kg mol^{-1}
M_n	molecular weight of species n, kg mol^{-1}
$m_{w,l}$	mass fraction of liquid water
$mass_n$	mass of species n, kg
n	number of electrons
n_d	electro-osmosis drag coefficient
$P^{sat}_{w,k}$	saturation vapor pressure of water in stream k, Pa
P	pressure, Pa
P_n	partial pressure of species n, Pa
R	universal gas constant, 8.314 J $(mol\ K)^{-1}$
r	condensation rate, s^{-1}
S	source term
t_f	liquid water film thickness, m
t_m	membrane thickness, m
T	temperature, K
V	velocity, m s^{-1}
V_{OC}	open circuit voltage, V
V_{cell}	cell voltage, V
W	width, m
$X_{i,k}$	mole fraction of species i in stream k

Greek symbols

α	net water flux per proton
β	permeability, m^2
ε	porosity of the gas diffusion layer
η	overpotential, V
λ	water content in the membrane
μ	dynamic viscosity, kg s m^{-2}
$\rho_{m,dry}$	density of the dry membrane, kg m^{-3}
ρ	density of the mixture, kg m^{-3}
σ_m	membrane conductivity, S m^{-1}
ξ	stoichiometric rate

Subscripts and superscripts

a	anode
avg	average
c	cathode
ch	channel
cv	control volume
e	electrochemical reaction
glif	gas liquid interface
H_2	hydrogen
K	anode or cathode
l	liquid
O_2	oxygen
reac	reacting
sat	saturated
v	vapor
ζ	dummy variable for direction x, y or z

facilitating the distribution of reactants in that area. Under conditions of high operating current density, however, oxygen molecules struggle to reach the reacting area, especially in the downstream portion of the channel.

The performance of PEMFCs also depends on various physical and electrochemical parameters. Recently, Tao et al. [10] and Min et al. [11] examined the sensitivity of a three-dimensional, non-isothermal model of a PEMFC to variations in 11 parameters. In their simulations, the parameters were linked so as to reflect the situation in real PEMFCs; hence, a variation of one parameter in the model that had a positive influence on the cell performance could lead to variations in other parameters that negatively affected the performance [11]. These studies showed that the cell performance was sensitive to variations in the transfer coefficient, exchange current density, water vapor diffusion coefficient, oxygen diffusion coefficient, GDL porosity, and membrane conductivity. However, other parameters, such as the stoichiometric rate, pressure and temperature, also influence the fuel cell performance [12], especially the diffusion of reactants to the reacting area. From a geometrical standpoint, the shoulder (bipolar plate) and channel configurations also influence the flow of reactants and have a marked effect on the fuel cell performance. Moreover, these geometrical parameters affect the inlet velocity at the anode and cathode [13]. Usually, the inlet velocities of the reactants into the channels are defined by the equation

$$V_{\text{in},K} = \frac{\xi_K I_{\text{avg}} R T_K}{nFPX_i} \frac{A_{\text{reac}}}{A_{\text{ch}}}, \quad (1)$$

where ξ is the stoichiometric rate, I_{avg} is the average current density, R is the molar gas constant, T is the temperature, n is the number of electrons, F is Faraday's constant, P is the pressure, X_i is the mole fraction of species i, and A_{reac} and A_{ch} are the reacting area and channel cross-sectional area, respectively. The subscript K refers to the anode or cathode. A higher inlet velocity facilitates passage of the reactants to the reacting area and leads to more uniform reaction in the cell. Modifying PEMFC geometrical parameters such as the channel width, shoulder width or reacting area leads to changes in the boundary conditions such as the reactant inlet velocities and mass flow rates. To date, however, most researchers have not reported the inlet velocities and flow rates of the respective channels, nor have they adequately defined the boundary conditions.

Changing the channel geometry or flow field design to a non-planar [14] or wave-like pattern [15] usually leads to an increase in the overall reacting area. In such cases, the reactant inlet flow increases and the cell performance is enhanced. Merida et al. [14] proposed new structural designs for PEMFCs, including a non-planar PEMFC that exhibited better performance than conventional PEMFCs, as well as describing details of manufacturing challenges. They suggested that extra care is needed when manufacturing non-planar membrane electrode assemblies (MEAs), in particular that an appropriate technique must be used to bond the MEA between the two conducting plates or the flow field must be redesigned to provide sufficient internal structural support. Kuo and Chen [15] showed that the gas flow velocity and convective heat transfer in PEMFCs could be improved by using a wave-like gas flow channel. Various aspects of PEMFCs can potentially be improved in order to boost their penetration into the commercial market for power generation. These include the structural integrity, cost, weight, size, shape and mass production scheme, as well as the power density. One approach to improving the performance of PEMFCs is to maintain the same boundary conditions for the same reacting area while reducing the shoulder width compared with the channel face width. The best option for achieving this is to deflect the MEA from shoulder to shoulder, as shown in Fig. 1b. By using this option, the face width increases (as occurs for a trapezoidal channel cross-section [9]) and more reactants diffuse through the GDL to the reacting area.

In the present study, we performed simulations of PEMFCs with a new design for the channel shoulder geometry, in which the MEA is deflected from shoulder to shoulder. This new geometry was designed to improve the reactant and temperature distributions over the cell and thus to improve the cell performance. The deflection of the MEA helped to increase the channel face width and reduce the shoulder width while maintaining the same reacting area

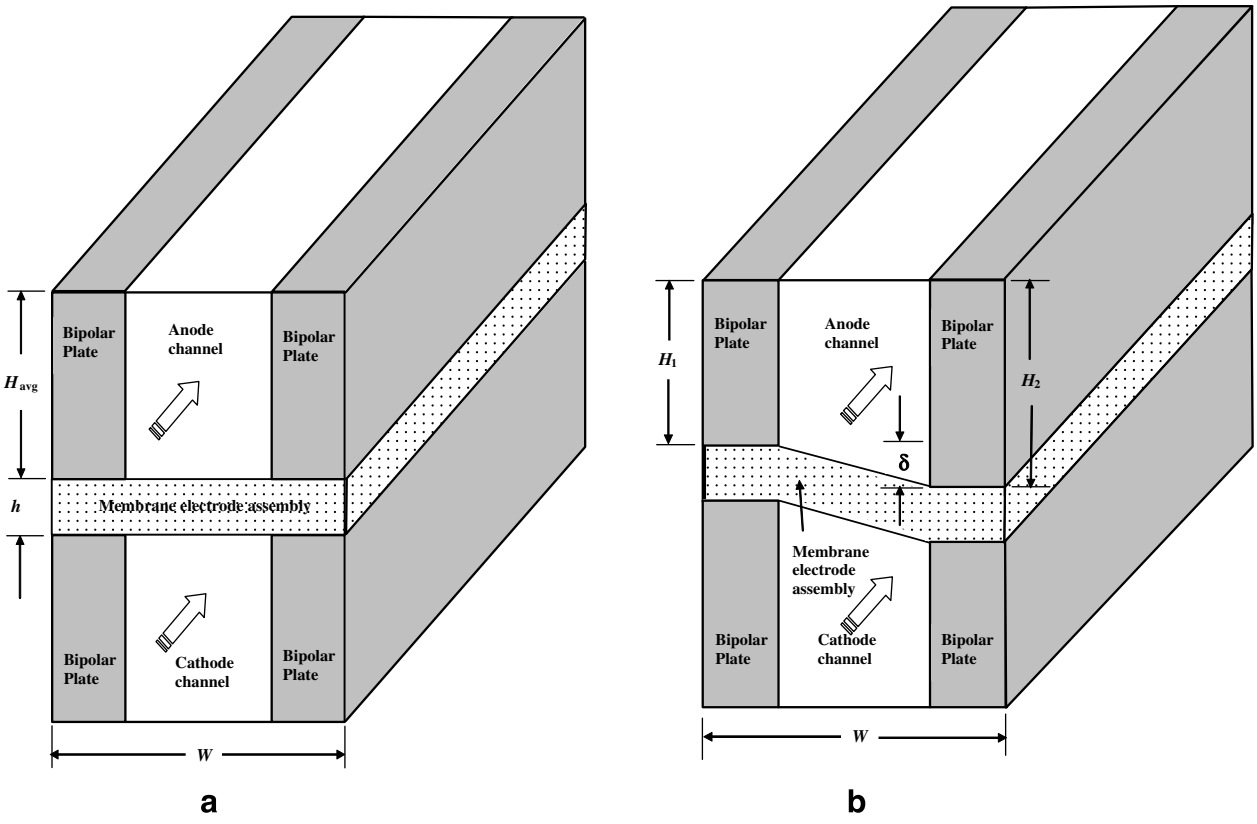

Fig. 1. (a) Conventional PEMFC geometry and (b) new PEMFC geometry with deflected MEA.

as for the system without any deflection. The performance of the cell with this new configuration was compared with that of the corresponding cell with the conventional channel shoulder geometry, in terms of characteristics such as local water and thermal management, local current density, and reactant distributions over the cell. A three-dimensional model with single straight channel geometry was employed for the computational analysis. In addition, the feasibility of deflecting the MEA was assessed by analyzing the bending characteristics of typical MEA materials under clamping pressures taken from the literature. The simulation results were validated by comparison with results in the literature.

2. Numerical simulation

A schematic diagram of a conventional PEMFC with a channel-to-shoulder width ratio of 1 is shown in Fig. 1. The system consists of two channels (for hydrogen and air) between which the membrane electrode assembly (MEA) is sandwiched. There are bipolar plates (also known as shoulders) on both the anode and cathode sides, which function as current collectors with high electronic conductivity. Humidified hydrogen and air are introduced into the respective channels, where the quantities of the two gases are determined by the stoichiometric rate and average current density, as in Eq. (1). The following assumptions are made in the model: ideal gas mixture, steady state, laminar flow, isotropic and homogeneous porous GDL, homogeneous two phase flow, and negligible potential drop in the bipolar plates.

The governing equations for the numerical simulation are conservation of mass, momentum transport, species transport, and energy equations.

(1) *Conservation of mass equation*

$$\nabla \cdot (\rho \vec{u}) = S_{m_a} + S_{m_c}. \tag{2}$$

The source terms are

$$S_{m_a} = S_{H_2} + S_{wv_p} + S_{w,l_p} + S_{awv_e}, \tag{2.1}$$

$$S_{m_c} = S_{O_2} + S_{wv_p} + S_{w,l_p} + S_{cwv_e}, \tag{2.2}$$

$$\text{where } S_{H_2} = -\frac{M_{H_2} A_{cv} I}{2F} \text{ and } S_{O_2} = -\frac{M_{O_2} A_{cv} I}{4F}. \tag{2.3}$$

The mass contributions of the water vapor at the anode and cathode sides are

$$S_{awv_e} = -\frac{M_{H_2O} A_{cv} \alpha I}{F}, \tag{2.4}$$

$$S_{cwv_e} = S_{cwv_t} + S_{cwv_p} = \frac{M_{H_2O} A_{cv} I}{2F} + \frac{\alpha M_{H_2O} A_{cv} I}{F} = \frac{(1+2\alpha) M_{H_2O} A_{cv} I}{2F}. \tag{2.5}$$

The change of phases between water vapor and liquid water depends on the partial pressure, and is defined as [16]

$$S_{w,l_p} = -S_{wv_p} = -\frac{M_{H_2O} \sum_{n\text{of v}} \frac{\text{mass}_{n\text{of v}}}{M_{n\text{of v}}}}{\left(1 - \frac{P_{wv}^{sat}}{P}\right)} \left[\frac{P_{wv}^{sat} - P_{wv}}{P}\right] * r, \tag{2.6}$$

where r is the condensation rate (set to 1 s^{-1} in the model). Eq. (2.6) shows that phase changes of water can be detected by monitoring the partial pressure of water vapor compared with the saturated pressure. Specifically, if the partial pressure of water vapor exceeds the saturated pressure, the water vapor will condense, whereas if the partial pressure of water vapor is lower than the saturated pressure, the liquid water will evaporate.

In Eqs. (2.4) and (2.5), α is the net water transfer coefficient per proton through the membrane, which is defined as

$$\alpha = n_d - \frac{F D_W [C_{wc} - C_{wa}]}{I t_m}. \tag{2.7}$$

Here, D_W is the water diffusion coefficient. The electro-osmotic drag coefficient (n_d) can be correlated with the membrane water content (λ) [17]:

$$n_d = 0.0029\lambda^2 + 0.05\lambda - 3.4 \times 10^{-19}. \tag{2.8}$$

(2) *Momentum transport equation*

$$\nabla \cdot (\rho \vec{u}\vec{u}) = -\nabla P + \nabla \cdot (\mu \nabla \vec{u}) + S_{p,i}, \tag{3}$$

where $S_{p,i}$ is the sink source term for porous media in the x-, y- and z-directions. The pressure drop in porous media can be accounted for using Darcy's law [18]. The source term is defined as

$$S_{p,i} = -\left(\sum_{j=1}^{3} \frac{1}{\beta_j} \mu u_j\right), \tag{3.1}$$

where β is the permeability.

(3) *General species transport equation*

$$\nabla \cdot (\rho m_n \vec{u}) = \nabla \cdot (J_n) + S_s, \tag{4}$$

where n denotes H_2, O_2, water vapor, or liquid water. The source terms are the same as those for the conservation of mass equation. The transportation of the species is solved with bulk mixture velocities and with diffusion mass fluxes. The diffusion mass flux of each species is evaluated with binary diffusion coefficients [19] and is reduced by 50% in the diffusion layer to account for the effect of the porosity and tortuosity of the pores [16]. It is assumed that the liquid water is in the form of small droplets freely suspended in the gas flow. This means that the two phases flow together (homogeneous two phase flow) under normal, steady-state operating conditions but not under supersaturated conditions. The diffusion mass flux (J) of species n in direction ζ is

$$J_{\zeta,n} = -\rho D_{\zeta,n} \frac{\partial m_{K,n}}{\partial \zeta}, \tag{4.1}$$

where ζ is a dummy variable for direction x, y or z.

(4) *Energy equation*

$$\nabla(\rho \vec{u} h) = \nabla \cdot (k \nabla T) + S_h. \tag{5}$$

The source term S_h contains contributions from energy losses and heat associated with phase transformations. The heat source from the electrochemical reaction is given by the difference between the total energy released by the electrochemical reaction at the cathode membrane surface and the electrical energy extracted out of the fuel cell [20]:

$$S_{h_e} = h_{rxn}\left[\frac{IA_{cv}}{2F}\right] - IV_{cell}A_{cv}. \tag{5.1}$$

The heat source due to a phase change can be expressed as

$$S_{h_p} = S_{w,l_p} * h_{fg}, \tag{5.2}$$

where h_{fg} is the enthalpy of formation of water. The local current density of the cell is calculated from the open circuit voltage (V_{OC}) and the losses

$$I = \frac{\sigma_m}{t_m}\{V_{OC} - V_{cell} - \eta\}, \tag{6}$$

which can be rewritten as

$$V_{cell} = V_{OC} - \eta - \frac{t_m}{\sigma_m}I. \tag{7}$$

The last term on the right hand side of Eq. (7) corresponds to the ohmic loss, where t_m is the membrane thickness and σ_m is the membrane conductivity, both of which are calculated as functions of the water content on the membrane surface at the anode interface. The membrane conductivity can be expressed as [16]

$$\sigma_m = \left(0.514\frac{M_{m,dry}}{\rho_{m,dry}}C_{wa} - 0.326\right)\exp\left(1268\left(\frac{1}{T_0} - \frac{1}{T}\right)\right), \tag{8}$$

where $T_0 = 303$ K. The water vapor concentration is defined as

$$C_{wa} = \frac{\rho_{m,dry}}{M_{m,dry}}\lambda, \tag{9}$$

where $\rho_{m,dry}$ and $M_{m,dry}$ are the material density and the equivalent weight of a dry proton electrode membrane, respectively. The water content in the membrane (λ) is defined as

$$\begin{aligned}\lambda &= (0.043 + 17.8a_K - 39.8a_K^2 + 36.0a_K^3) \quad \text{if } a_K \leqslant 1,\\ \lambda &= (14 + 1.4(a_K - 1)) \quad \text{if } a_K > 1,\end{aligned} \tag{10}$$

where the subscript K stands for the anode or cathode. a_a is the water activity and is defined as

$$a_a = \frac{X_{w,a}P}{P^{sat}_{w,a}}, \tag{11}$$

where P is the cell pressure and $X_{w,a}$ is the mole fraction of water on the anode side $P^{sat}_{w,a}$ is the saturation pressure of anode water. The local overpotential (η) for a PEMFC is included for both the anode overpotential (AOP) and cathode overpotential (COP) and can be written as [21]

$$\eta = \frac{RT}{\alpha_c F}\ln\left[\frac{IP}{I_{0_{O_2}}P_{O_2}}\right] + \frac{RT}{\alpha_a F}\ln\left[\frac{IP}{I_{0_{H_2}}P_{H_2}}\right], \tag{12}$$

where P is the pressure, α_a and α_c are the transfer coefficients for the anode and cathode, respectively, and I_0 is the exchange current density. The partial pressure is calculated as $P_{O_2} = X_{O_2}P$, and $P_{H_2} = X_{H_2}P$. Here, X_{O_2} and X_{H_2} are the oxygen and hydrogen mole fractions, respectively. By including the partial pressure, the overpotential terms also include the activation and concentration overpotentials.

In the present model, the source terms of different conservation equations correspond to the control volume, not to the boundary conditions of the anode or cathode interface. To determine the concentrations and activities at the membrane–GDL interface correctly, the mole fraction of each species is extrapolated to the membrane surface. This extrapolation procedure is not, however, performed when a liquid water film is generated on the membrane surface. If liquid water is present at the MEA, the model accounts for the mass transfer resistance of the gas diffusing through the film of water. To achieve this, Henry's Law is used to calculate the solubility of the reactants in the liquid water film [20]. The diffusion length of the dissolved gas is determined by the thickness of the film of water on the MEA corrected for the porosity of the GDL. Moreover, the average pore flooding is accounted for by considering an average film thickness:

$$\begin{aligned}-\frac{I}{4F}M_{O_2} &= \rho_{O_2}D_{O_2,l}\left[\frac{X_{O_2,glif}P_{glif}H^{-1}_{O_2,l} - X_{O_2}}{t_{f,c}}\right],\\ -\frac{I}{2F}M_{H_2} &= \rho_{H_2}D_{H_2,l}\left[\frac{X_{H_2,glif}P_{glif}H^{-1}_{H_2,l} - X_{H_2}}{t_{f,a}}\right],\end{aligned} \tag{13}$$

where P_{glif} is the pressure at the gas–liquid water interface, H is the Henry constant of the reactants in the liquid water film, and $t_{f,K}$ is the liquid water film thickness for the anode or cathode, which is defined as

$$t_{f,K} = \frac{m_{w,l}(\sum \text{mass}_n)}{\varepsilon\rho_{w,l}\text{Area}_{cv}}. \tag{14}$$

Here, ε is the porosity of the GDL, $m_{w,l}$ is the liquid water mass fraction at the membrane–GDL interface, and mass_n is the mass of species n. The above governing equations are solved using appropriate boundary conditions. The SIMPLE algorithm is used to solve the above equations. The numbers of cells (62,976) are used in the present study, which is enough to fulfill the convergence criterion for the single unit fuel cell. To obtain the stability, computations efficiency and accuracy of the simulation results, the model is computed for double precision. In addition, the mass balance is up to 0.1% for simulations.

3. Design of the deflected membrane electrode assembly

In conventional PEMFCs, the channels for the anode and cathode are straight with a serpentine or integrated

flow field and the MEA is in a single plane. The conventional single straight channel geometry with a channel-to-shoulder width ratio of 1 is shown in Fig. 1a, and our new concept of a channel flow field with a deflected (non-planar) MEA is shown in Fig. 1b. The major feature distinguishing the proposed geometry from the conventional one is that whereas the heights of the two pairs of adjacent shoulders (ribs) of the anode and cathode channels are the same in the conventional geometry, they differ in the proposed geometry. As a result, the MEA, which consists of a gas diffusion electrode (GDE) and membrane, is deflected according to the difference in height between the shoulders of the anode or cathode channel. In the present study, we define the difference in height between the two adjacent shoulders of the anode or cathode channel as the 'deflection' (δ), where $\delta = H_2 - H_1$, as shown in Fig. 2. The average height of the anode or cathode channel will therefore be $H_{avg} = (H_1 + H_2)/2$, which is the same as in the conventional geometry (see Fig. 1). A major aspect of the present study is that the reacting area is kept the same as in the base case (no deflection), which ensures the same reactant flow rates and boundary conditions for all cases. To achieve this, the shoulder widths of the deflected MEA are reduced according to the deflection of the MEA. This means that the face width (channel face width) is increased compared with the base case of no deflection. As a result, the width of MEA is kept to be the same (MEA width = channel face width + shoulder width). This ensures that the reacting areas are the same for all the deflection cases. The relevant geometrical parameters of the different cases are listed in Table 1.

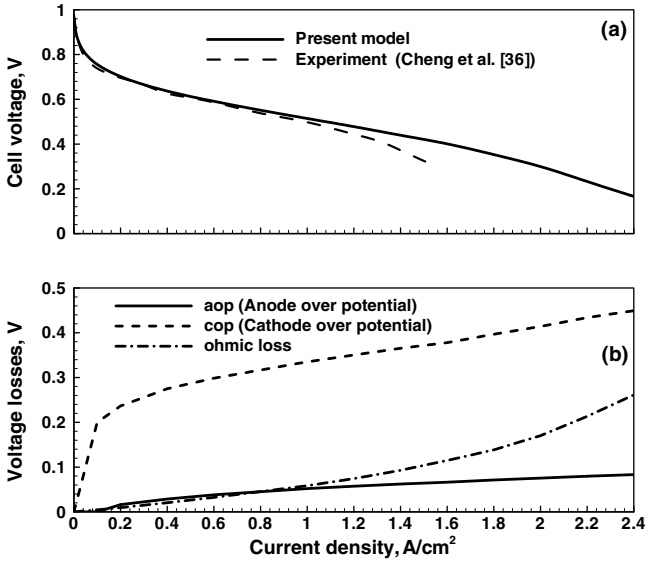

Fig. 2. (a) Polarization curve and (b) different types of voltage loss. (See above-mentioned references for further information.)

Table 1
Different deflection case studies with related channel-to-shoulder width ratio

Deflection (δ), mm	δ/H_{avg}	Channel width (W_{ch}), mm	Channel face width ($W_{Ch,f}$), mm	Half shoulder width (Sh/2), mm	Ch:Sh
0.0 (no deflection)	0.0	0.8	0.8	0.4	1:1
0.4	0.4	0.8	0.89443	0.35279	1:1.2677
0.6	0.6	0.8	1	0.3	1:1.67
0.8	0.8	0.8	1.1314	0.2343	1:2.4142
1.0	1.0	0.8	1.2806	0.1597	1:40,098

4. Results and discussion

A series of simulations were carried out on the base case (no deflection) from low operating current density to high operating current density; the geometrical and physical parameters for the base case are listed in Tables 2 and 3, respectively. The polarization curve for the base case, shown in Fig. 2a, shows three distinct regions of losses. The variations in the different overpotentials or losses as a function of operating current density, shown in Fig. 2b, also follow the typical trend for conventional PEMFCs

Table 2
Geometrical parameters

Parameter	Value (mm)
Channel length	34.7
Channel width	0.8
Channel height	1
Membrane length	31.7
Membrane thickness	0.05
Anode gas diffusion layer	0.25
Cathode gas diffusion layer	0.25

Table 3
Physical and electrochemical parameters

Parameter	Value
Anode pressure	1 atm
Cathode pressure	1 atm
Stoichiometric rate at anode	1.2
Stoichiometric rate at cathode	2.0
Cell temperature	70 °C
Anode inlet temperature	80 °C
Cathode inlet temperature	70 °C
Open circuit voltage	0.96 V
Relative humidity at anode	100%
Relative humidity at cathode	100%
Oxygen inlet mole fraction	0.146
Oxygen exchange current density	200 A m^{-2}
Hydrogen exchange current density	2000 A m^{-2}
Anode transfer coefficient	1.2
Cathode transfer coefficient	0.6
Porosity	0.7
Permeability	1×10^{-12} m^2
Anode top surface temperature (z-direction)	70 °C
Cathode top surface temperature (z-direction)	70 °C

[10]. It should be noted that the ohmic loss in Fig. 2b shows a non-linear trend rather than the linear trend reported in the literature because the present model was implemented with variable membrane conductivity.

In order to investigate the performance of cells with the proposed geometry, we studied four deflection cases ($\delta = 0.4$, 0.6, 0.8 and 1.0 mm) as well as the base case without deflection ($\delta = 0.0$ mm). Conventional PEMFCs show poor cell performance at high current density due to concentration losses or mass transport limitations. In the present study of the cell performance and the related discussion, we concentrate on high current density operation (2.4 A cm^{-2}). In the remainder of this paper, we consider the systems in terms of the deflection (δ) normalized by the average channel height (H_{avg}),δ/H_{avg}. After this normalization, the four deflection cases considered here are $\delta/H_{avg} = 0.4$, 0.6, 0.8, and 1.0. The cell voltages for the different deflection cases at an operating current density of 2.4 A cm^{-2} are shown in Fig. 3. It is clearly observed that the cell performance increases with increasing δ/H_{avg} (and increase of the channel–shoulder width ratio (see Table 1)) up to $\delta/H_{avg} = 0.6$, but decreases for $\delta/H_{avg} > 0.6$. This observation indicates that for a certain channel–shoulder width ratio, a certain degree of deflection improves the cell performance but too great a deflection degrades the performance.

The local current density distributions at the membrane–cathode GDE interface for the various deflection cases are shown in Fig. 4. At the high operating current density considered here ($I_{avg} = 2.4$ A cm^{-2}), the local current density is high at the channel–shoulder interface for all deflection cases, which is consistent with previous results for conventional PEMFCs obtained by our group [22] and others [23]. The improvement of the local current density distribution, especially at the shoulder area, for the cells with higher deflections can be attributed to the easy access of the reactants to the shoulder region in these systems. In confirmation of this hypothesis, the oxygen mass fraction distribution at the membrane–cathode GDE interface is significantly improved for the higher deflection cases, as shown in Fig. 5. However, it is important to note

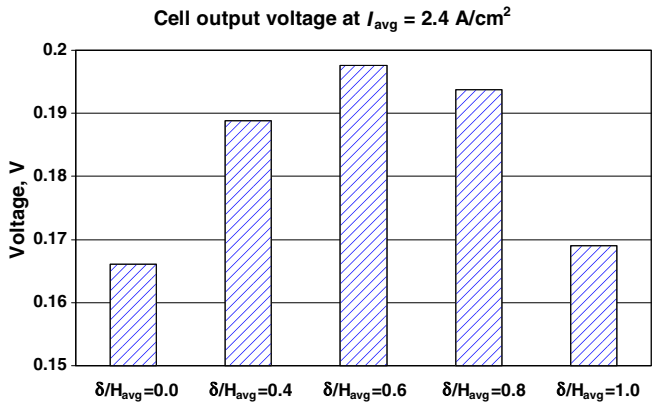

Fig. 3. Output cell voltage at an operating current density of 2.4 A cm^{-2}.

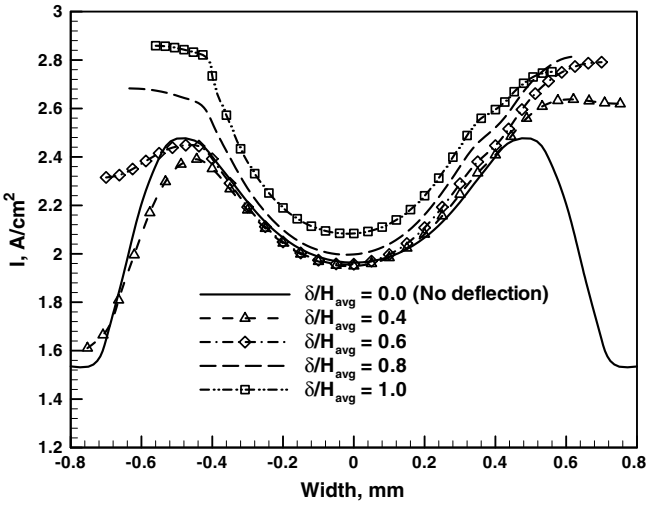

Fig. 4. Local current density distribution for different deflection cases at an operating current density of 2.4 A cm^{-2}.

that the variation of the oxygen mass fraction in the two shoulder regions (width in the positive direction and width in the negative direction in Fig. 5) depends strongly on the deflection (δ). In the deflected systems, the higher oxygen mass fraction in the width in the positive direction arises from the lower shoulder height at the cathode side, which makes it easier for the reactants to diffuse through the GDL. The temperature distributions at the membrane–cathode GDE interface for the various deflection cases are shown in Fig. 6. This result indicates that a uniform temperature distribution can be obtained even when the membrane is deflected. The reason for this is that the fixed temperature is set for the bipolar plate, which has good thermal conductivity. The AOPs and COPs along the width are shown in Figs. 7 and 8, respectively. The COP decreases markedly at higher δ/H_{avg}, especially in the shoulder region. The reduction in COP can be attributed

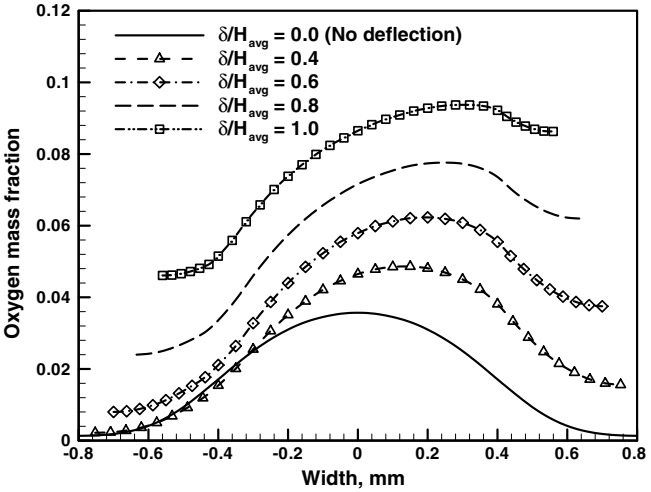

Fig. 5. Oxygen mass fraction distributions at the membrane–cathode GDE interface.

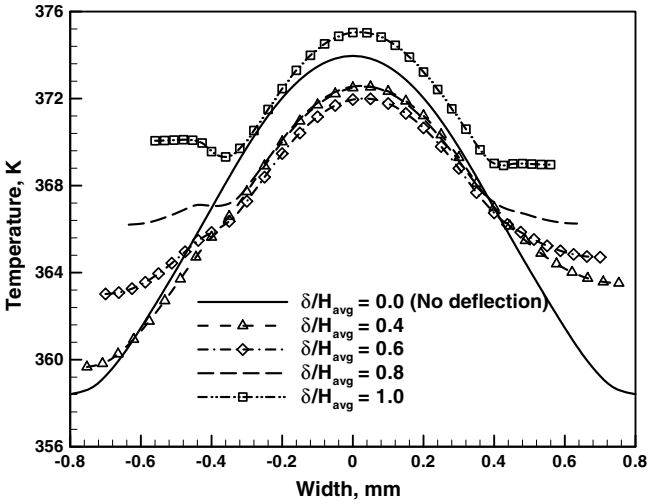

Fig. 6. Local temperature distributions at the membrane–cathode GDE interface.

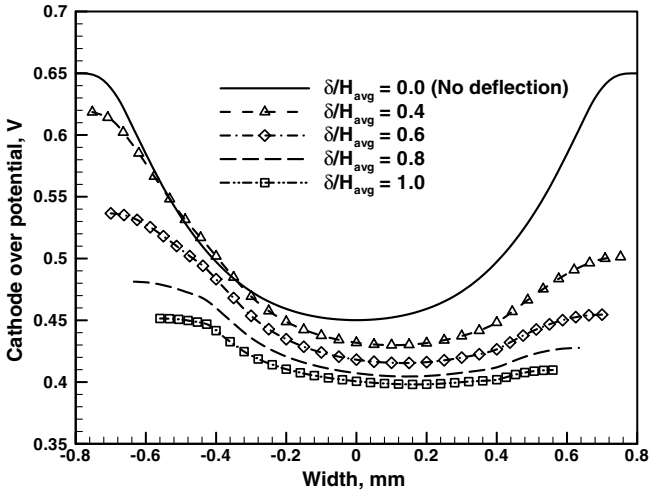

Fig. 8. Cathode overpotential distributions at the membrane–cathode GDE interface.

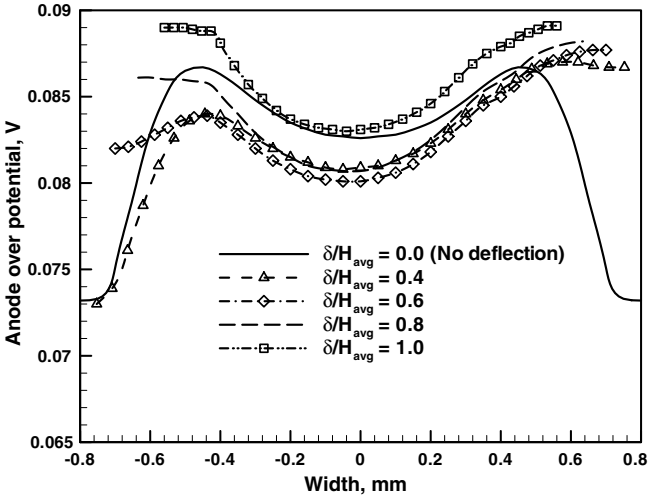

Fig. 7. Anode overpotential distributions at the membrane–anode GDE interface.

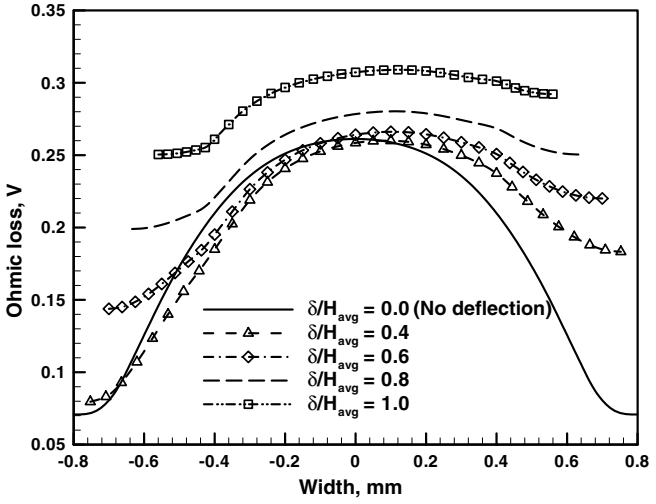

Fig. 9. Ohmic overpotential distributions at the membrane–cathode GDE interface.

to better and more uniform reactant distributions over the reacting area at higher deflections, as shown for the oxygen mass fraction in Fig. 5. On the other hand, the ohmic overpotential (see Fig. 9) is higher at higher values of δ/H_{avg}. When larger quantities of reactants diffuse through the GDL to the reacting area, the local membrane conductivity decreases [4]. As a consequence, the ohmic overpotential increases with increasing δ/H_{avg}. The local membrane conductivity profile at the membrane–cathode GDE interface is shown in Fig. 10. Lessening the membrane conductivity specially in the shoulder region can be attributed to the higher reactant availability (see Fig. 5) which cases more chemical reaction over the reacting area in systems with higher δ/H_{avg}. Furthermore, membrane conductivity depends on anode water activity and temperature distribution as shown in Eq. (8). In general, at high operating current density, a much greater quantity of reactants are involved in the chemical reaction and a larger amount of water is dragged from the anode to the cathode by electro-osmosis. The anode water activity at the membrane–anode GDE interface is shown in Fig. 11 for the various δ/H_{avg} cases. A comparison of the losses (AOP, COP, and ohmic overpotential) for the different δ/H_{avg} cases is shown in Fig. 12. The AOP is relatively insensitive to deflection of the membrane, whereas the COP decreases as δ/H_{avg} increases. However, significant reduction of COP is observed for smaller δ/H_{avg} but further increase of δ/H_{avg} does not help to reduce COP remarkably. On the contrary, the ohmic overpotential gradually increases with increasing δ/H_{avg}. Considering the different trends in the losses, the maximum output cell voltage is obtained at a δ/H_{avg} of around 0.6, which corresponds to a channel-to-shoulder width ratio of around 1.67.

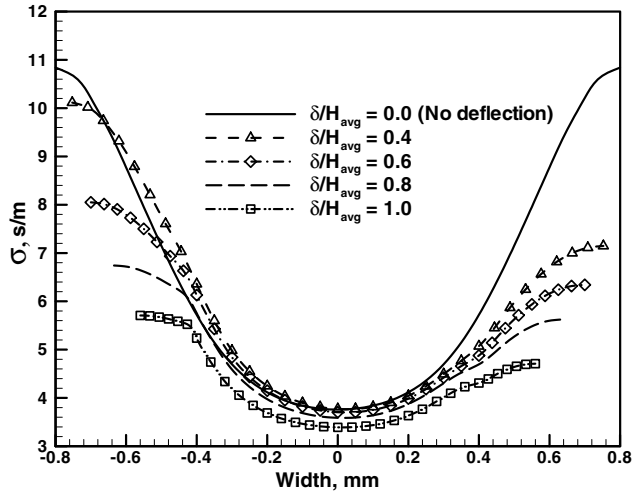

Fig. 10. Membrane conductivity distributions at the membrane–cathode GDE interface.

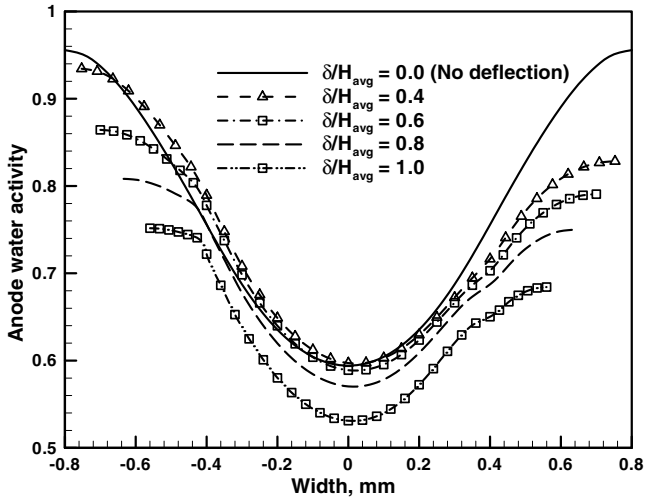

Fig. 11. Anode water activity at the membrane–anode GDE interface.

5. Related technical issues

The major components of a fuel cell stack are the bipolar plates and the MEA, which constitute almost 90% of the total cost of the cell [24,25]. Furthermore, the bipolar plates account for about 80% of the total weight and 45% of the stack cost [25]. The major advantages of the cell geometry proposed in the present work are that it allows the size and weight of the fuel cell to be reduced (as the shoulder width is reduced to maintain the same reacting area and boundary conditions), and also reduces the materials costs of the bipolar plates. In addition, the cell performance is significantly improved for δ/H_{avg} around 0.6, which corresponds to a channel-to-shoulder width ratio of around 1.67. For this condition, a uniform local current density distribution is obtained throughout the cell. Moreover, a less variation of temperature in the cell is achieved, which is essential to avoid thermal distortion of the fuel cell.

A major concern regarding the proposed geometry is whether the deflection leads to degradation of the physical and chemical properties of the MEA. Since the heights of the two adjacent shoulders are different, the membrane and GDE properties will be affected after long periods of operation. As a result, the cell performance may be reduced in practical situations. Every material can bend or deflect to some extent when a force is applied. When the applied force is within the elastic limit of a material, there are usually no changes in its internal properties. The bending or deflection of the different material components of the MEA can be calculated for a given clamping pressure or force and the related material properties are available in the literature [26–29] and are shown in Table 4. The area of the surface to which the force is applied is calculated according to the dimensions labeled in Fig. 13. The deflection can be varied by varying the clamping force, although too high a clamping force may damage the GDE and membrane materials. In the present calculation, we only consid-

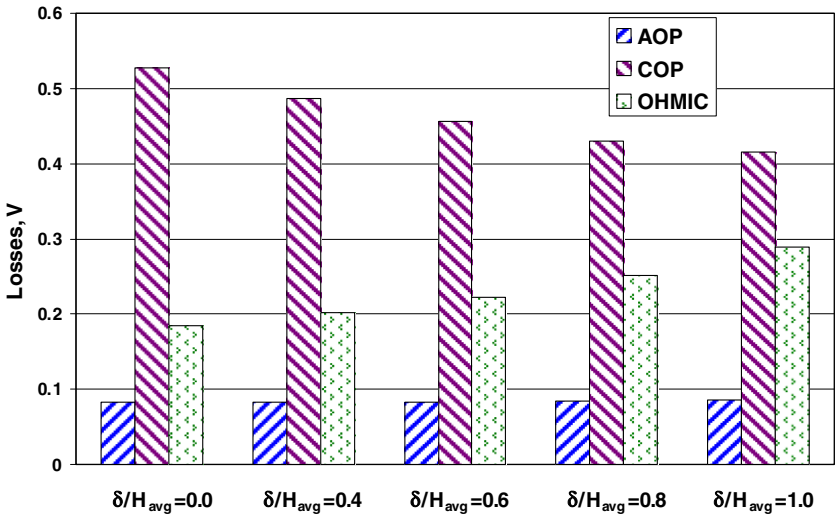

Fig. 12. Comparison of different overpotentials.

Table 4
Calculated deflections of different MEA materials from the literature

Length, l, m	Width, b, m	Height, h, m	Area ($l \times b$), m^2	Applied clamping pressure, Pa	Applied clamping force, N	Modulus of elasticity, Pa	Moment of inertia, m^4	Deflection, mm
0.0032	0.0317	0.00025	0.00010144	3E+06 [26,27]	304	1.00E+10 (GDE) [28]	4.1276E−14	0.503
0.0032	0.0317	0.00005	0.00010144			2.49E+08 (membrane) [28]	3.3021E−16	2526.689
0.0032	0.0317	0.00025	0.00010144	5W+05 [26,27]	50.7	1.00E+10 (GDE) [28]	4.1276E−14	0.083886
0.0032	0.0317	0.00005	0.00010144			2.49E+08 (membrane) [28]	3.3021E−16	421.1149
0.0032	0.0317	0.00025	0.00010144	3.75E+06	380 [29]	1.00E+10 (GDE) [28]	4.1276E−14	0.628
0.0032	0.0317	0.00005	0.00010144			2.49E+08 (membrane) [28]	3.3021E−16	3155.04

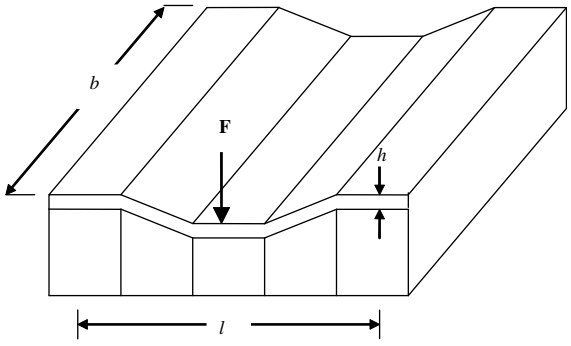

Fig. 13. Schematic diagram for deflection calculation.

ered clamping pressures (available from the literature) that are within the yield strength limit of the MEA materials. The yield strength and tensile strength of different fuel cell components vary depending on the manufacturer and the production process used. For example, E-TEK division cites the tensile strength of the gas diffusion electrode (GDE) LT 250E-W as around 0.225 MPa and the gas diffusion layer (GDL) LT 2500-W as around 0.22 MPa [30], while GRAFCELL® cites the tensile strength and compressive yield strength for its gas diffusion electrodes as wide ranges of 0.5–2 MPa and 1–5 MPa, respectively [31]. In the case of membranes, the yield strength varies over the range of 3–7 MPa or more depending on the temperature, water swelling, thickness, and so on [32,33]. Table 4 indicates that under a given clamping pressure, the GDE is deflected to a much lesser degree than the membrane due to the brittle nature of the former [34]. Hence, the membrane can easily sustain the clamping forces and allow sufficient deflection within its elastic limit. It has been reported that the Nafion® membrane is characterized by high tenacity and toughness [32], and that Nafion 117 has no effect on elongation at break [35]. Moreover, the chemical properties and chemical bond of HSO_3 groups and their hydrophobic and hydrophilic properties, water swelling and temperature dependency are much more sensitive for the membrane than for the GDE. On the other hand, the physical properties of GDEs (or layers), in particular the permeability and porosity, are more important than the chemical properties because they affect the diffusion of the reactants to the catalyst layer. However, the applied clamping pressures taken from the literature that we have used in the present deflection calculations are close to the elastic limit of the GDE. Furthermore, the optimum deflection we obtained in the present numerical study also falls within the calculated deflections shown in Table 4. It should be noted here that the dimensions of the system (from Fig. 13) significantly affect the results of the deflection calculation. For example, in Fig. 13, if $l = 0.004$ m is used instead of the value of 0.0032 m to obtain the results in Table 4 ($l = 0.004$ will correspond to a channel width of 1 mm and a channel-to-shoulder width ratio of 1), the deflections of the GDE will be 1.2288, 0.2048 and 1.2275 mm for clamping pressures of 3, 0.5 and 3.75 MPa, respectively. From a physical (mechanical) viewpoint, the membrane and GDE can be used in their deflected (non-planar) states provided the applied clamping pressure is less than the elastic limit (yield strength). However, during long-term operation, the chemical properties and performance of a fuel cell may vary. Thus, detailed experimental investigations of the mechanical and chemical properties of fuel cells during long-term operation are required, so as to examine the effect on cell performance of different MEA deflections. Moreover, research should be conducted on the chemical properties of membranes and GDEs under deflection or non-planar conditions.

6. Conclusions

In the present study, we carried out numerical simulations of PEMFCs with a single straight channel geometry in which the MEA was deflected from shoulder to shoulder. In the present examination of cells with a deflected MEA, the major aim was to examine the effect on the cell performance of reducing the shoulder width while maintaining the same reacting area and boundary conditions. Numerical simulations showed that the cell performance increased with increasing δ/H_{avg} (ratio of deflection to average channel height) and channel-to-shoulder width

ratio. However, the cell performance deteriorated when δ/H_{avg} was increased beyond 0.6. The simulation results also revealed that the reactants diffused uniformly over the reacting area though the GDL, and hence uniform local current density was obtained in these deflected cells. The results also showed that a less variation of temperature in the cell was achieved for larger deflections of the MEA. In addition, the COP decreased significantly for higher deflections of the MEA, leading to an improvement in the cell performance. We further performed calculations to examine the deflection of different MEA materials under clamping pressures taken from the literature. This preliminary analysis showed that the different materials of the MEA could be deflected up to the optimum deflection for clamping pressures within the elastic limit of the GDE. Taken together, our findings indicate that use of a deflected MEA in PEMFCs can improve the cell performance while also affording other advantages such as reduced materials costs, weight, and size.

References

[1] D. Natarajan, T.V. Nguyen, A two-dimensional, two-phase, multicomponent, transient model for the cathode of a proton exchange membrane fuel cell using conventional gas distributors, J. Electrochem. Soc. 148 (12) (2001) A1324–A1335.

[2] G. Lin, T.V. Nguyen, A two-dimensional two-phase model of a PEM fuel cell, J. Electrochem. Soc. 153 (2) (2006) A372–A382.

[3] K.W. Lum, J.J. McGuirk, Three-dimensional model of a complete polymer electrolyte membrane fuel cell – model formulation, validation and parametric studies, J. Power Sour. 143 (2005) 103–124.

[4] D.H. Ahmed, H.J. Sung, Effects of channel geometrical configuration and shoulder width on PEMFC performance at high current density, J. Power Sour. 162 (2006) 327–339.

[5] F.-B. Weng, A. Su, G.-B. Jung, Y.-C. Chiu, S.-H. Chan, Numerical prediction of concentration and current distributions in PEMFC, J. Power Sour. 145 (2005) 546–554.

[6] S. Shimpalee, W.K. Lee, J.W. Van Zee, H.N. Neshat, Predicting the transient response of a serpentine flow-field PEMFC I. Excess of normal fuel and air, J. Power Sour. 156 (2006) 355–368.

[7] H.C. Liu, W.M. Yan, C.Y. Soong, F. Chen, Effects of baffle-blocked flow channel on reactant transport and cell performance of a proton exchange membrane fuel cell, J. Power Sour. 142 (2005) 125–133.

[8] H.C. Liu, W.M. Yan, C.Y. Soong, F. Chen, H.S. Chu, Reactant gas transport and cell performance of proton exchange membrane fuel cells with tapered flow field design, J. Power Sour. 158 (2006) 78–87.

[9] L. Sun, P.H. Oosthuizen, K.B. McAuley, A numerical study of channel-to-channel flow cross-over through the gas diffusion layer in a PEM-fuel-cell flow system using a serpentine channel with a trapezoidal cross-sectional shape, Int. J. Thermal Sci. 45 (2006) 1012–1026.

[10] W.Q. Tao, C.H. Min, X.L. Liu, Y.L. He, B.H. Yin, W. Jiang, Parameter sensitivity examination and discussion of PEM fuel cell simulation model validation: Part 1. Current status of modeling research and model development, J. Power Sour. 160 (2006) 359–373.

[11] C.H. Min, Y.L. He, X.L. Liu, B.H. Yin, W. Jiang, W.Q. Tao, Parameter sensitivity examination and discussion of PEM fuel cell simulation model validation: Part 2. Results of sensitivity analysis and validation of the model, J. Power Sour. 160 (2006) 374–385.

[12] C.R. Tsai, F. Chen, A.C. Ruo, M.H. Chang, H.S. Chu, C.Y. Soong, W.M. Yan, C.H. Cheng, An analytical solution for transport of oxygen in cathode gas diffusion layer of PEMFC, J. Power Sour. 160 (2006) 50–56.

[13] S. Um, C.-Y. Wang, K.S. Chen, Computational fluid dynamics modeling of proton exchange membrane fuel cells, J. Electrochem. Soc. 147 (12) (2000) 4485–4493.

[14] W.R. Merida, G. McLean, N. Djilali, Non-planner architecture for proton exchange membrane fuel cells, J. Power Sour. 102 (2001) 178–185.

[15] J.K. Kuo, C.K. Chen, Evaluating the enhanced performance of a novel wave-like form gas flow channel in the PEMFC using the field synergy principle, J. Power Sour., doi: 10.1016/j.jpowsour.2006.07.053.

[16] S. Dutta, S. Shimpalee, J.W. Van Zee, Three-dimensional numerical simulation of straight channel PEM fuel cells, J. Appl. Electrochem. 30 (2000) 135–146.

[17] T.E. Springer, T.A. Zawodzinski, S. Gottesfeld, Polymer electrolyte fuel cell model, J. Electrochem. Soc. 138 (8) (1991) 2334–2342.

[18] R.B. Bird, W. Stewart, E. Lightfoot, Transport Phenomena, Wiley, New York, 1960.

[19] J.C. Slattery, R.B. Bird, Calculation of the diffusion coefficient of dilute gases and of the self-diffusion coefficient of dense gases, AIChE J. 4 (1958) 137–142.

[20] STAR-CD Version 3.24 methodology, CD-Adapco Group.

[21] S. Shimpalee, S. Dutta, Numerical prediction of temperature distribution in PEM fuel cells, Numer. Heat Transfer A 38 (2000) 111–128.

[22] D.H. Ahmed, H.J. Sung, Local current density and water management in PEMFCs, Int. J. Heat Mass Transfer. 50 (2007) 3376–3389.

[23] H. Meng, C.Y. Wang, Electron transport in PEFCs, J. Electrochem. Soc. 151 (3) (2004) A358–A367.

[24] X. Yan, M. Hou, H. Zhang, F. Jing, P. Ming, B. Yi, Performance of PEMFC stack using expanded graphite bipolar plates, J. Power Sour. 160 (2006) 252–257.

[25] H. Tsuchiya, O. Kobayashi, Mass production cost of PEM fuel cell by learning curve, Int. J. Hydr. Energy 29 (2004) 985–990.

[26] P. Zhou, C.W. Wu, G.J. Ma, Contact resistance prediction and structure optimization of bipolar plates, J. Power Sour. 159 (2006) 1115–1122.

[27] V. Mishra, F. Yang, R. Pitchumani, Measurement and prediction of electrical contact resistance between gas diffusion layers and bipolar plate for applications to PEM fuel cells, J. Fuel Cell Sci. Technol., Trans. ASME 1 (2004) 2–9.

[28] Y. Tang, M.H. Santare, A.M. Karlsson, S. Cleghorn, W.B. Johnson, Stresses in proton exchange membranes due to hygro-thermal loading, J. Fuel Cell Sci. Technol. 3 (2006) 119–124.

[29] K. Wikander, H. Ekstrom, A.E.C. Palmqvist, A. Lundblad, K. Holmberg, G. Lindbergh, Alternative catalysts and carbon support material for PEMFC, J. Fuel Cell 6 (6) (2006) 21–25.

[30] <http://www.etek-inc.com/standard/index.php>.

[31] <www.grafcell.com>.

[32] A. Mian, G. Newaz, L. Vendra, X. Wu, S. Liu, Role of defects on mechanical response of Nafion® membranes for fuel cell applications, in: Second International Conference on Fuel Cell Science, Engineering and Technology, June 14–16, 2004, Rochester, NY, USA.

[33] K. Tang, A.M. Karlsson, M.H. Santare, M. Gilbert, S. Cleghorn, W.B. Johnson, An experimental investigation of humidity and temperature effects on the mechanical properties of perfluorosulfonic acid membrane, Mater. Sci. Eng. A 425 (2006) 297–304.

[34] S.J. Lee, C.D. Hsu, C.H. Huang, Analyses of the fuel cell stack assembly pressure, J. Power Sour. 145 (2005) 353–361.

[35] Y. Gao, G.P. Robertson, M.D. Guiver, S.D. Mikhailenko, X. Li, S. Kalianuine, Low-swelling proton-conducting copoly (aryl ether nitrile)s containing naphthalene structure with sulfonic acid groups *meta* to the ether linkage, Polymer 47 (2006) 808–816.

[36] B. Cheng, O. Minggao, Y. Baolian, Analysis of water management in proton exchange membrane fuel cells, Tsing. Sci. Technol. 11 (1) (2006) 54–64.